

RADIOACTIVE SCANDIUM IN THE YOUNGEST GALACTIC SUPERNOVA REMNANT G1.9+0.3

KAZIMIERZ J. BORKOWSKI,¹ STEPHEN P. REYNOLDS,¹ DAVID A. GREEN,² UNA HWANG,³ ROBERT PETRE,³ KALYANI KRISHNAMURTHY,⁴ & REBECCA WILLETT⁴

ABSTRACT

We report the discovery of thermal X-ray emission from the youngest Galactic supernova remnant G1.9+0.3, from a 237-ks *Chandra* observation. We detect strong $K\alpha$ lines of Si, S, Ar, Ca, and Fe. In addition, we detect a 4.1 keV line with 99.971% confidence which we attribute to ^{44}Sc , produced by electron capture from ^{44}Ti . Combining the data with our earlier *Chandra* observation allows us to detect the line in two regions independently. For a remnant age of 100 yr, our measured total line strength indicates synthesis of $(1-7) \times 10^{-5} M_{\odot}$ of ^{44}Ti , in the range predicted for both Type Ia and core-collapse supernovae, but somewhat smaller than the $2 \times 10^{-4} M_{\odot}$ reported for Cas A. The line spectrum indicates supersolar abundances. The Fe emission has a width of about $28,000 \text{ km s}^{-1}$, consistent with an age of ~ 100 yr and with the inferred mean shock velocity of $14,000 \text{ km s}^{-1}$ deduced assuming a distance of 8.5 kpc. Most thermal emission comes from regions of lower X-ray but higher radio surface brightness. Deeper observations should allow more detailed spatial mapping of ^{44}Sc , with significant implications for models of nucleosynthesis in Type Ia supernovae.

Subject headings: ISM: individual objects (G1.9+0.3) — ISM: supernova remnants — nuclear reactions, nucleosynthesis, abundances — X-rays: ISM

1. INTRODUCTION

The supernova remnant (SNR) G1.9+0.3 has an age of order 100 years (Reynolds et al. 2008, Paper I; Green et al. 2008). Its integrated X-ray spectrum is well described by a model of synchrotron emission from a power-law distribution with an exponential cutoff (XSPEC model `srcut`), with rolloff frequency $h\nu_{\text{roll}} = 2.2 \text{ keV}$ and a very high absorbing column density $N_H \cong 5 \times 10^{22} \text{ cm}^{-2}$ (Reynolds et al. 2009, Paper II). The high column suggests a distance of order that to the Galactic Center; we adopt a nominal distance of 8.5 kpc, at which the mean expansion rate is $v_s \sim 14,000 \text{ km s}^{-1}$ (Paper I). No thermal emission is apparent in the integrated spectrum based on short (50 ks in duration) *Chandra* observations in early 2007. Without the detection of thermal emission, basic, crucial information such as the supernova (SN) type, distance, and elemental abundances cannot be obtained. Its detection was one of the goals of a much longer *Chandra* observation.

2. OBSERVATIONS

We re-observed G1.9+0.3 for 237 ks with *Chandra* in four observations between July 13 and 26, 2009, using the ACIS-S CCD camera (S3 chip). We checked aspect correction and created new level-1 event files appropriate for VFAINT mode. No flares occurred during the observation. CTI correction was applied and calibration was performed using CALDB version 3.4.0. Finally, the datasets were merged and weighted response files created. We extracted spectra using the `specextract` script. We obtained about 40,000 source counts.

Figure 1 shows the 2009 image, smoothed with the spatio-spectral method of Krishnamurthy et al. (2010). Figure 2 compares the radio and X-ray morphologies. The marked and

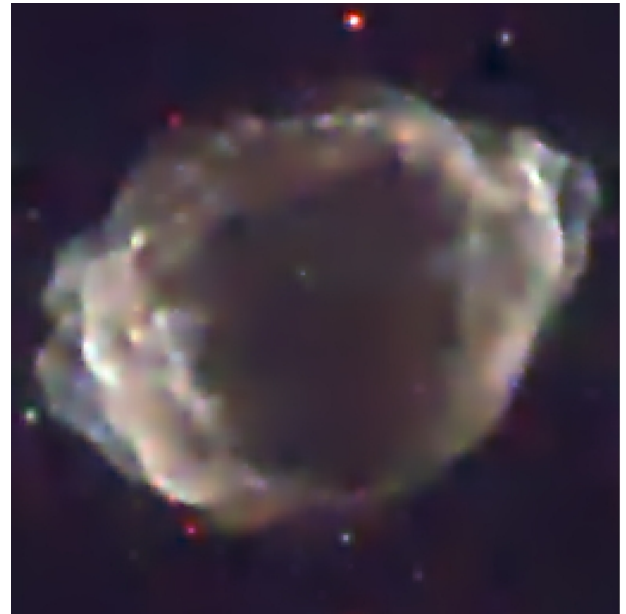


Figure 1. *Chandra* image of G1.9+0.3. Red, 1 – 3 keV; green, 3 – 4.5 keV; blue, 4.5 – 7.5 keV. Image size $127'' \times 121''$.

surprising difference between them, particularly strong radio but weak X-rays in the north, suggests that the radio image may hold a clue to the location of thermal emission. We extracted the spectrum from the radio-bright region shown on Figure 2; it is shown in Figure 3. Lines are apparent. We found lines as well in the central region shown in Figure 2, and analyzed the regions separately.

3. SPECTRAL ANALYSIS

We combined the 2007 and 2009 datasets for a total exposure of 286 ks. We modeled the background rather than subtracting it, and used Markov chain Monte Carlo (MCMC) methods as implemented in the PyMC software package (Patil et al. 2010) to determine best parameter values and error ranges (e.g., van Dyk et al. 2001). MCMC methods require

¹ Department of Physics, North Carolina State University, Raleigh, NC 27695-8202; kborkow@unity.ncsu.edu

² Cavendish Laboratory; 19 J.J. Thomson Ave., Cambridge CB3 0HE, UK

³ NASA/GSFC, Code 660, Greenbelt, MD 20771

⁴ Department of Electrical and Computer Engineering, Duke University, Durham, NC 27708

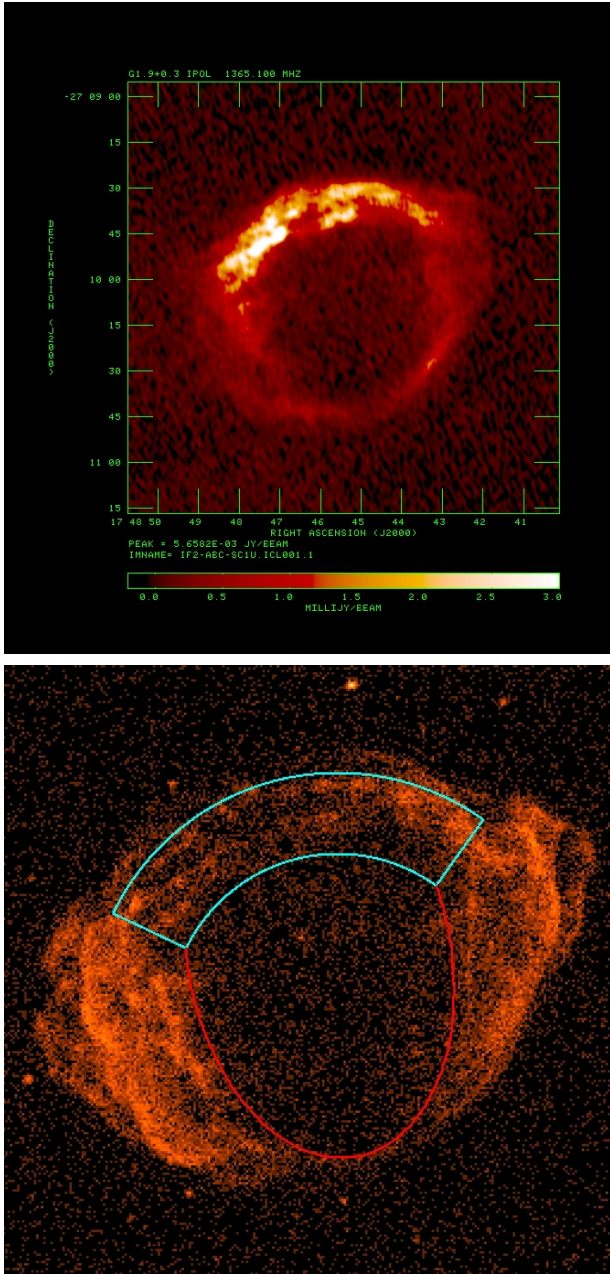


Figure 2. Top: 1.4 GHz radio image (Green et al. 2010, in preparation). Resolution $2.3'' \times 1.4''$. Bottom: X-ray image showing regions from which spectra below were extracted. Blue: North rim. Red: center.

the specification of priors on parameters to be determined (as described below).

The spectrum of the northern, radio-bright rim is shown in the upper panel of Figure 3. Spectral lines typical of strongly underionized plasma are apparent (such plasma is expected in G1.9+0.3 because of its youth and the low density of the ambient ISM). SN 1006 has a very similar X-ray spectrum; in the same spectral range of Figure 3, Yamaguchi et al. (2008) find prominent $K\alpha$ lines of abundant elements such as Si, S, Ar, Ca, and Fe, with line centroids at 1.815 keV, 2.36 keV, 3.01 keV, 3.69 keV, and 6.43 keV. (As in SN 1006, O, Ne, and Mg lines might also be present at lower energies, but cannot be seen because of the high absorption.) In addition to these lines produced in hot shocked plasma, the radioactive decay of ^{44}Ti to ^{44}Sc and finally to the stable isotope ^{44}Ca will result

in the emission of X-ray and γ -ray lines in very young remnants (^{44}Ti decays with a mean life of 85.0 ± 0.4 yr, Ahmad et al. 2006). This decay commences via an electron capture to ^{44}Sc , leaving a K-shell vacancy followed rapidly either by Auger decay or by emission of a fluorescence photon of energy 4.09 keV (the yield is 0.172 photons per each ^{44}Ti decay; Bé et al. 2004). Nuclear de-excitation Sc γ -ray lines at 78.4 and 67.9 keV are also emitted, followed by Ca gamma rays at 1.157 MeV (mean life of ^{44}Sc is 5.4 hr). An inspection of the radio-bright rim spectrum (Figure 3) reveals the presence of Si, S, Ar, and Fe $K\alpha$ lines, and a broad feature near 4 keV that may be a blend of Doppler-broadened Ca and Sc $K\alpha$ lines. Lines are generally weaker in the low-surface brightness interior (lower panel of Figure 3), with Ar and Sc lines being the most prominent.

We modeled the spectra of the northern, radio-bright rim and the faint interior with an absorbed power law plus emission lines of Si, S, Ar, Ca, Sc, and Fe. This simple model does not account for dust scattering and does not separate the underlying continuum into thermal and nonthermal components, but it suffices for the determination of line strengths, centroids, and widths. We used a normal (Gaussian) prior for the absorbing column density N_H , with mean (standard deviation) of $6.89(0.11) \times 10^{22} \text{ cm}^{-2}$, based on our multi-region spectral fit without dust scattering to the 2007 data (Paper II). (Solar abundances of the absorbing ISM are those of Grevesse & Sauval 1998; fits with dust scattering resulted in N_H lower by 25%.) Noninformative, uniform and logarithmic priors were assumed for the power-law index Γ and the (unabsorbed) 5–10 keV continuum flux $F_{5-10 \text{ keV}}$, respectively.

We used normal priors for line energies, setting mean thermal line energies equal to the values measured by Yamaguchi et al. (2008) for SN 1006, and to 4.09 keV for the Sc line. In view of the $14,000 \text{ km s}^{-1}$ blast wave speed, significant bulk Doppler shifts are possible, so we chose a large ($\sigma = 10^4 \text{ km s}^{-1}$) width for these priors. (For numerical stability, these normal priors were truncated to include only a finite range in line energies; we verified that our results are not affected by this procedure.) Thermal lines in a young remnant arise in a fast-moving, shocked shell bounded by forward and reverse shocks. An optically and geometrically thin shell expanding with velocity v_{shell} produces flat-topped lines with Doppler widths of $2v_{shell}$. We assumed flat-topped profiles with the same (but unknown) Doppler width for all thermal lines. (Thermal broadening is likely of only modest importance, $(kT_i/m_i)^{1/2} \sim 0.2v_{shell}$, based on models of Dwarkadas & Chevalier (1998) with exponential ejecta density profiles. But it may still be appreciable in off-center locations such as the north rim, where bulk radial motions contribute less to the line broadening.) A truncated normal prior was assumed for v_{shell} , with mean of $14,000 \text{ km s}^{-1}$ and 1σ width of 5000 km s^{-1} , extending from 0 to $50,000 \text{ km s}^{-1}$. The Sc line was modeled by a Gaussian with width σ_v^{Sc} ; we assumed a half-normal⁵ prior with $\sigma = 0.15 \text{ keV}$ for σ_v^{Sc} . These priors for line widths exclude very large ($> 50,000 \text{ km s}^{-1}$) widths, but otherwise provide weak constraints.

Some constraints on the Sc line strength are provided by IBIS/ISGRi onboard INTEGRAL. The 68 and 78 keV lines have been detected by IBIS/ISGRi in Cas A (Renaud et al. 2006) but not in G1.9+0.3 (Renaud et al. 2009). We use the Cas A detection to bound priors. We chose a weakly informative gamma prior for the Sc line strength, defined as the

⁵ normal distribution with mean 0 limited to positive domain

expected line counts in a 286 ks exposure with *Chandra*, with shape parameter $\alpha = 1.2$ and scale parameter $\beta = 0.01$ (see van Dyk et al. (2001) for discussion of the use of gamma priors in modeling emission lines in X-ray spectra). Its mean of $\alpha/\beta = 120$ counts is comparable to the square root of the variance, equal to $(\alpha/\beta^2)^{1/2} = 110$ counts. This prior disfavors a strong Sc line that was searched for but not found in Cas A (Theiling & Leising 2006), but otherwise provides rather weak constraints. We assumed the same weakly informative prior on line strength for thermal lines of Si, S, Ar, Ca, and Fe.

The sky background was determined by a fit to the background spectrum extracted from a large area on the S3 chip. The sky background was modeled by two absorbed power-laws, while the particle background model involved a combination of power-laws with exponential cutoffs and narrow fluorescent lines. We allowed for spatial variations in the particle background, with a logarithmic prior imposed on the particle normalization.

Table 1 contains results of spectral fits; models are plotted in Figure 3. Except for fluxes, values quoted in Table 1 are standard means of the MCMC draws. We used a geometric mean for $F_{5-10 \text{ keV}}$, and mean line fluxes F were evaluated as $(\langle F^{1/2} \rangle)^2$ (according to recommendations by van Dyk et al. 2001). The 90% confidence intervals were computed using the 0.05 and 0.95 quantiles of the draws. The Sc line width is poorly constrained, so we provide only upper limits based on the 90% highest probability density interval for σ_v^{Sc} .

The Sc line and thermal lines of all abundant elements have appreciable strengths in the spectrum of the northern rim. Thermal lines are very broad, with a full width of 28,000 km s⁻¹, consistent with the estimated shock velocity of 14,000 km s⁻¹. The Fe K α line provides the strongest constraints on line widths, but Doppler broadening is important for other lines as well. Photon statistics are insufficient to study variations in Doppler widths between different elements. This includes Sc, with a width that does not seem to be different from thermal line widths. But Sc forms a line blend with Ca, so errors are particularly large for these elements. In the interior, thermal lines are much weaker; an inspection of the confidence intervals in Table 1 suggests that only Ar may have been unambiguously detected. Notwithstanding this decline in the overall strength of thermal lines, the Sc line remains strong (it is only a factor of 2 weaker than in the northern rim). The prominence of Sc in the interior is consistent with an origin in the unshocked ejecta.

In both spectral regions independently, we examined the significance of the Sc line detection using a likelihood ratio test as described in Protassov et al. (2002). The null model consisted of an absorbed power law plus Si, S, Ar, Ca and Fe lines described by flat line profiles with equal (but unknown) Doppler widths, together with the same priors that we used for our spectral fits. The alternative model is obtained by adding an additional line at 4.09 keV to the null model. Large samples from the posterior distribution of the null model were obtained using MCMC simulations. From these samples we simulated synthetic datasets, fit each dataset with the null model and the alternative model, and computed the likelihood ratio statistic. The posterior predictive p -values for the null model are 0.0098 and 0.030 for the northern rim and interior, respectively. The p -value is equal to 0.00029 for the null model to be valid in both of these regions. We can therefore reject the null model, i.e., claim the detection of the 4.1 keV line, at 99.971% significance.

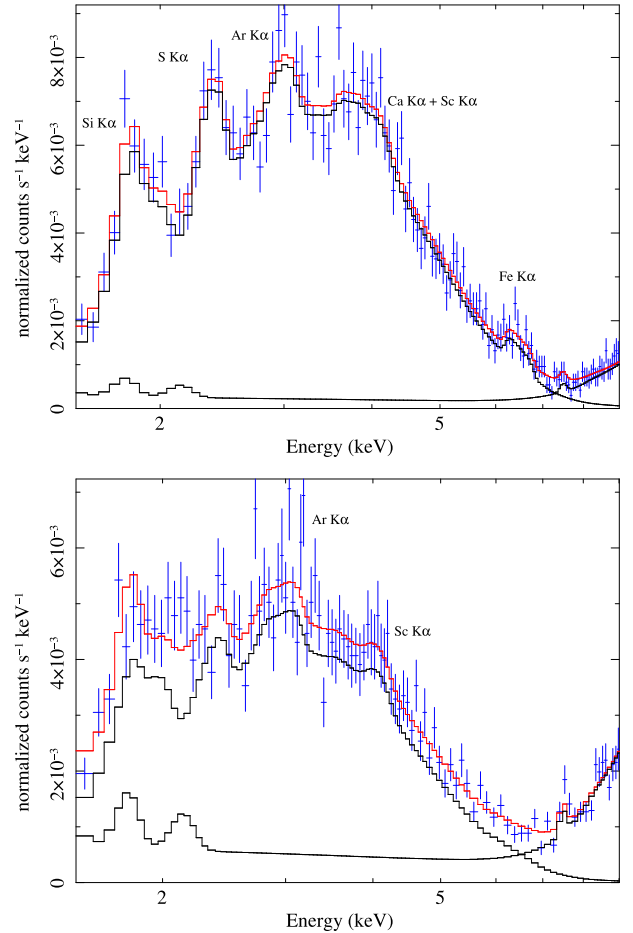


Figure 3. Top: Spectrum of N rim (radio-bright region) shown in Figure 2. Lines of Ca and Sc blend together because of the large Doppler widths. Bottom: Spectrum of interior region. In both cases, background has been modeled rather than subtracted; source and background models are described in the text. The two black lines are the background and source models; the red line is the total.

The total Sc line flux was derived by combining the spectra shown in Figure 3, and fitting the combined dataset separately with the same spectral model as before. We obtain a total Sc line flux of $1.2 \times 10^{-6} \text{ ph cm}^{-2} \text{ s}^{-1}$, with a 95% confidence interval of $(0.35, 2.4) \times 10^{-6} \text{ ph cm}^{-2} \text{ s}^{-1}$. The column density of $6.9 \times 10^{22} \text{ cm}^{-2}$ implies that X-rays of 4.1 keV are attenuated by about 33% due both to absorption and scattering. The Sc line fluxes have not been corrected for this, but the correction has been made for the ⁴⁴Ti masses that are discussed next.

We expect 0.172 fluorescence photons per ⁴⁴Sc atom. Thus the line flux, along with the source age and distance, gives directly the amount of ⁴⁴Ti synthesized in the explosion. Including the branching ratio for the emission of the 1.157 MeV photon, we expect the flux of X-ray photons to be related to that in 1.157 MeV photons by $F_x = 0.15F_\gamma$. The gamma-ray flux is related to the mass of ⁴⁴Ti by

$$F_\gamma = 3.6 \times 10^{-6} \frac{M(\text{Ti})}{10^{-5} M_\odot} \left(\frac{D}{8.5 \text{ kpc}} \right)^{-2} \left(\frac{\tau}{\text{yr}} \right)^{-1} e^{-t/\tau} \text{ ph cm}^{-2} \text{ s}^{-1}$$

with the mean life $\tau = 85$ yr. (If the ⁴⁴Ti is ionized beyond the He-like state, the effective lifetime is longer (Mochizuki et al. 1999), but the low ionization age of Fe implied by the line centroid reported in Table 1 means that this effect should be negligible.) We used these relations with an age of 100 yr

to obtain the following ^{44}Ti masses: $2.8(1.1, 5.1) \times 10^{-5} M_{\odot}$ in the north, $1.3(0.36, 2.6) \times 10^{-5} M_{\odot}$ in the interior, and $3.3(0.95, 6.5) \times 10^{-5} M_{\odot}$ for the total. (Errors are 90% confidence limits for the two subregions, but 95% limits for the total.) These masses have been corrected for absorption and scattering by being multiplied by a factor of 3/2. For an age of 140 yr (corresponding to no deceleration at all), the masses would be larger by an additional factor of 1.54.

We also modeled the spectrum of the northern, radio-bright rim with a plane shock non-equilibrium ionization (NEI) model (`vpshock` in XSPEC). We find $N_H = 6.88(6.72, 7.03) \times 10^{22} \text{ cm}^{-2}$; $kT_e = 3.6 \pm 0.4 \text{ keV}$; and ionization timescale $\tau \equiv n_e t = 1.4(0.78, 3.1) \times 10^9 \text{ cm}^{-3} \text{ s}$. This extremely low ionization age is very unusual for SNRs, but appropriate for an unprecedentedly young object. Abundances have substantial errors, but solar abundances are ruled out: compared to solar, Si (set equal to S) = 3.4 (2.0, 4.6), Ar = 17 (2.8, 37), and Fe = 4.1(2.4, 5.7). A blueshift of line centers is required, $v_r = -4,300(-7,600, -1,300) \text{ km s}^{-1}$. We find a FWHM of $26,500(17,600, 34,600) \text{ km s}^{-1}$. With $n_e \sim 2\tau/100 \text{ yr} = 0.7 \text{ cm}^{-3}$, the estimated shocked ejecta mass is only $\sim 0.016 M_{\odot}$, with comparable masses of intermediate-mass (Si, S, and Ar) elements and Fe. This is a quarter of the total shocked ambient gas mass of $0.06 M_{\odot}$ (for a preshock density of $\sim 0.04 \text{ cm}^{-3}$ and a blast wave radius of 2.2 pc; Paper I). Impact of the ejecta with a denser than average ambient medium in the north may explain the relatively high shocked ejecta mass and density, and the strong radio emission there.

4. DISCUSSION

We summarize our results as follows:

1. The radio-bright N rim region shows strong $K\alpha$ lines of Si, S, Ar, Ca, and Fe (much weaker thermal emission is also present in the shell interior).
2. The spectral lines are both broadened and shifted. Widths of thermal lines are $28,000 \pm 5,000 \text{ km s}^{-1}$ with blueshifts of about $4,000 \text{ km s}^{-1}$.
3. Global spectral fits with a plane-shock model imply strong overabundances of the elements we detect, consistent with their interpretation as ejecta dominated by intermediate-mass elements and Fe.
4. We detect for the first time with high significance a line at 4.1 keV which we attribute to ^{44}Sc . The line strength of about $1.2 \times 10^{-6} \text{ ph cm}^{-2} \text{ s}^{-1}$ implies a mass of ^{44}Ti of $3.3(0.95, 6.5) \times 10^{-5} M_{\odot}$, after correction for absorption and assuming an age of 100 yr and a distance of 8.5 kpc.
5. We detect ^{44}Sc separately in the northern shell and the interior, with greater strength in the shell.

We believe the discovery of ^{44}Sc emission to be the most important new result. A feature at 4.1 keV identified with ^{44}Sc has been reported previously in G266.2–1.2 (RX J0852.0–4622) by Tsunemi et al. (2000), Iyudin et al. (2005), and Bamba et al. (2005). However, Slane et al. (2001) and, more comprehensively, Hiraga et al. (2009) have failed to confirm these reports, at a level below the previous detection claims. It appears that G1.9+0.3 shows the first definite detection of this transition. Our line strength implies a flux in the 1.157 MeV line of about $1.2 \times 10^{-5} \text{ ph cm}^{-2} \text{ s}^{-1}$, well below the COMPTEL limit of about $2 \times 10^{-5} \text{ ph cm}^{-2} \text{ s}^{-1}$ (Dupraz et al. 1997).

While our inferred ^{44}Ti mass is nominally in conflict with the upper limit of $2 \times 10^{-5} M_{\odot}$ reported by Renaud et al. (2009), the errors are large enough to accommodate it.

^{44}Ti , a trace product of explosive nucleosynthesis, carries important information about the details of the explosion (Diehl & Timmes 1998; The et al. 2006). It is primarily produced in “ α -rich freezeout” conditions, in which rapid cooling causes departures from nuclear statistical equilibrium and a high concentration of free α particles. In core-collapse (CC) SNe, its production is sensitive to the location of the mass cut (within which material becomes the neutron star), and in most models its production is correlated with that of ^{56}Ni , and therefore with the supernova luminosity. Predicted yields range from 3 to $9 \times 10^{-5} M_{\odot}$ (see summary in The et al. 2006). Traditional SN Ia models undergo α -rich freezeout under somewhat different conditions and do not produce large quantities of ^{44}Ti . However, recent simulations of off-center delayed-detonation explosions have shown substantially increased yields: Maeda et al. (2010) quote a mass of ^{44}Ti of $1.6 \times 10^{-5} M_{\odot}$, compared to $2 \times 10^{-6} M_{\odot}$ for a centrally-ignited pure deflagration and $3 \times 10^{-6} M_{\odot}$ for a central delayed detonation. (For comparison, the benchmark W7 Type Ia model [Nomoto et al. 1984] gives $8 \times 10^{-6} M_{\odot}$, while a series of more recent simulations by Iwamoto et al. (1999) gives a range from $(1-5) \times 10^{-5} M_{\odot}$.)

Galactic constraints on the supernova rate can be obtained from the observed abundance of ^{44}Ca , and the absence of obvious discrete sources of 1.157 MeV γ -ray emission, with the important exception of Cas A, the only firm detection to date (Iyudin et al. 1994, 1999). The accompanying hard X-ray lines have also been seen from Cas A (Vink et al. 2001; Renaud et al. 2006), with an inferred mass of ^{44}Ti of about $2 \times 10^{-4} M_{\odot}$, more than expected from most CC models ($(6-14) \times 10^{-5} M_{\odot}$; Timmes et al. 1996), though asymmetric models can do better (e.g., Nagataki et al. 1998).

Since the 4.1 keV inner-shell transition of ^{44}Sc formed from electron capture in ^{44}Ti does not require that the scandium be ionized, we are sensitive to both shocked and unshocked material. This is evident in the interior spectrum in Figure 3, in which the ^{44}Sc line is as prominent as in the north rim, but the other lines are weaker. The greater abundance of ^{44}Sc in the north, then, represents a true spatial distribution – surprising, considering that the ^{44}Sc is expected to be produced in the neighborhood of the Fe-peak elements, that is, the innermost ejecta. These properties suggest that the explosion was substantially asymmetric, perhaps consistent with the greater production of ^{44}Ti found in asymmetric explosion models such as Maeda et al. (2010). While He-shell denotations that trigger sub-Chandrasekhar thermonuclear explosions can also be invoked to explain the presence of asymmetrically-distributed ^{44}Ti and Fe in the outermost ejecta layers, too much ^{44}Ti is produced even in sub-Chandrasekhar explosion models with minimum He shell masses (Fink et al. 2010). A substantially longer observation should allow better spatial localization of the ^{44}Sc emission, and an unprecedented view into supernova nucleosynthesis.

Our discovery of these spectral lines, and the ^{44}Sc line in particular, remains consistent with the possibility that G1.9+0.3 resulted from a Type Ia event, a possibility we find increasingly likely. The bilaterally symmetric synchrotron–X-ray morphology, the extremely high shock velocities we both infer and measure from line broadening, and the prominent Fe K emission, all support a Type Ia origin. We have not yet ruled out a CC origin, however; while strong iron emission

Table 1
 Spectral Fits

Region	N_H (10^{22} cm $^{-2}$)	Γ	F_{5-10} keV (10^{-13} ergs cm $^{-2}$ s $^{-1}$)	v_{shell} (10^4 km s $^{-1}$)	σ_v^{Sc}	Line energies (keV) and line strengths (10^{-7} ph cm $^{-2}$ s $^{-1}$)					
						Silicon	Sulfur	Argon	Calcium	Scandium	Iron
North rim	6.88 (6.72, 7.05)	2.40 (2.29, 2.51)	3.00 (2.80, 3.22)	1.4 (0.9, 1.9)	1.1 < 1.9	1.83 (1.78, 1.88)	2.35 (2.31, 2.40)	2.99 (2.92, 3.04)	3.72 (3.59, 3.87)	4.08 (4.00, 4.15)	6.49 (6.38, 6.61)
Interior	6.89 (6.72, 7.06)	2.71 (2.54, 2.86)	1.35 (1.22, 1.51)	2.1 (1.2, 3.0)	0.9 < 1.6	1.83 (1.72, 1.95)	2.32 (2.17, 2.46)	2.96 (2.87, 3.05)	3.74 (3.52, 3.94)	4.09 (4.02, 4.17)	6.4 (6.0, 6.8)
						4.4 (2.1, 7.0)	10.4 (5.9, 15.6)	7.7 (3.1, 13)	5.2 (1.2, 11)	10 (4.0, 19)	18 (11, 27)
						1.2 (0.1, 4.0)	3.1 (0.4, 8.3)	5.9 (1.5, 13)	1.9 (0.2, 6.0)	4.6 (1.3, 9.5)	3.0 (0.4, 8.4)

Note. — Line energies (strengths) are in rows 1 and 5 (3 and 7), with 90% confidence limits listed in adjacent rows.

is unusual in CC remnants, Cas A is a counterexample, and it is possible that a CC origin can explain the other features as well. What is certainly clear is that G1.9+0.3 still has a great deal to teach us about the evolution of very young SNRs and about the supernovae that produced them.

This work was supported by NASA through Chandra General Observer Program grant SAO GO6-7059X.

REFERENCES

- Ahmad, I., et al. 2006, *Phys. Rev. C*, 74, 065803
 Bamba, A., Yamazaki, R., & Hiraga, J. S. 2005, *ApJ*, 632, 294
 Bé, M.-M., et al. 2004, *Table of Radionuclides*, Vol. 1, Monographie Bureau International des Poids et Mesures (BIMP-5), 51
 Diehl, R., & Timmes, F. X. 1998, *PASP*, 110, 637
 Dupraz, C., et al. 1997, *A&A*, 324, 683
 Dwarkadas, V. V., & Chevalier, R. A. 1998, *ApJ*, 497, 807
 Fink, M., et al. 2010, *A&A*, 514, A53
 Green, D. A., et al. 2008, *MNRAS*, 387, L54
 Grevesse, N., & Sauval, A. J. 1998, *Space Science Reviews*, 85, 161
 Hiraga, J. S., et al. 2009, *PASJ*, 61, 275
 Iwamoto, K., et al. 1999, *ApJS*, 125, 439
 Iyudin, A. F., et al. 1994, *A&A*, 284, L1
 Iyudin, A. F., et al. 1999, *Astrophys. Lett. Comm.*, 38, 383
 Iyudin, A. F., et al. 2005, *A&A*, 429, 225
 Krishnamurthy, K., Raginsky, M., & Willett, R. 2010, *SIAM J. Imaging Sci.*, 3, 619
 Maeda, K., et al. 2010, *ApJ*, 712, 624
 Mochizuki, Y., et al. 1999, *A&A*, 346, 831
 Nagataki, S., et al. 1998, *ApJ*, 492, L45
 Nomoto, K., Thielemann, F.-K., & Yokoi, K. 1984, *ApJ*, 286, 644
 Patil, A., et al. 2010, *J. of Statistical Software*, 35, Issue 4
 Protassov, R., et al. 2002, *ApJ*, 571, 545
 Renaud, M., et al. 2006, *ApJ*, 647, L41
 Renaud, M., et al. 2009, in *Proceedings of the 2nd International Symbol-X Symposium, Symbol-X: Focusing on the Hard X-ray Universe*. AIP Conf. Proc., 1126, 359
 Reynolds, S. P., et al. 2008, *ApJ*, 680, L41 (Paper I)
 Reynolds, S. P., et al. 2009, *ApJ*, 695, L149 (Paper II)
 Slane, P. O., et al. 2001, *ApJ*, 548, 814
 The, L.-S., et al. 2006, *A&A*, 450, 1037
 Theiling, M. F., & Leising, M., D. 2006, *New Astronomy Reviews*, 50, 544
 Timmes, F. X., et al. 1996, *ApJ*, 464, 332
 Tsunemi, H., et al. 2000, *PASJ*, 52, 887
 van Dyk, D. A., et al. 2001, *ApJ*, 548, 224
 Vink, J., et al. 2001, *ApJ*, 560, L79
 Yamaguchi, H., et al. 2008, *PASJ*, 60, 141